The Local Aerosol Emission Effect on Surface Shortwave Radiation and Temperatures

The Local Aerosol Emission Effect on Surface Shortwave Radiation and Temperatures

N. Freychet[1], S. F. B. Tett[1], M. Bollasina[1], K.C. Wang[2], and G. C. Hegerl[1]

[1]School of Geosciences, University of Edinburgh, UK
[2]Beijing Normal University, Beijing, China

Key Points:

- Nudged simulation (1982-2016) is used to force the model dynamics and isolate the effect of aerosol emissions from the circulation feedback.
- The effect of aerosol emissions on temperatures over China is weak, possibly due to lower AOD changes (compared to Europe) and overshadowed by effects related to meteorology.
- Other regions (Europe, US and India) have more consistent response between radiation and temperatures. The effect on precipitation is however very limited.

This article has been accepted for publication and undergone full peer review but has not been through the copyediting, typesetting, pagination and proofreading process, which may lead to differences between this version and the Version of Record. Please cite this article as doi: 10.1029/2018MS001530

Corresponding author: Nicolas Freychet, Crew Building, The Kings Buildings, Alexander Crum Brown Road, Edinburgh, EH9 3FF (Nicolas.Freychet@ed.ac.uk)

Abstract

The local aerosol emissions effect is investigated by comparing two numerical simulations (1982-2016) with the UK HadGEM3-GA6 model nudged to the same ERA-Interim circulation. One includes full historical CMIP5 RCP4.5 aerosol emission changes while the second uses a monthly aerosol climatology from 1982. At global scale, the emission scenario does not change the mean surface energy balance but it shows strong regional contrasts. Thus we focus on regions where the change in emission has been the largest: North America, Europe, India and China.

No clear impact on temperature trends is found over China although aerosol emissions have increased in recent decades. This could be explained by a stronger role of meteorology in this region rather than direct surface heating, and also by a more limited change in AOD compared to regions such as Europe. Other regions show clearer responses to aerosol effect, consistent with previous studies: Cooler maximum temperatures (with historical emission compared to fixed emissions) where emissions have increased (North-East of India) and warmer maximum temperatures where emissions have decreased (Europe). However, in each region, the interannual variability in temperatures is strongly controlled by the circulation. Precipitation is also locally decreased (0.5 mm.day^{-1}) over North India during summer due to a reduction of moisture convergence in the boundary layer (where no nudging is applied).

Based on these simulations, we suggest that radiation-driven aerosol emission impacts on local surface temperature and precipitation is not linear and can be mitigated or cancelled by the local dynamics.

1 Introduction

Climate change projections depend on understanding key factors affecting the climate system and how they are represented (or not) in the current climate models. Among these factors, aerosols have remained the dominant contributor to the uncertainty in radiative forcing and our ability to estimate their contribution to the recent global temperature change is limited (Gillett, Arora, Matthews, & Allen, 2013; Ribes & Terray, 2013; Stott & Jones, 2012). The effect of aerosols on the surface radiative forcing is complex. The direct aerosol effect is to absorb and scatter solar radiation (Twomey, 1991) and thus to decrease the downward shortwave radiation at the surface (SSR). The principal indirect effect is to alter the clouds albedo and lifetime (Boucher et al., 2013) which is, also, expected to reduce SSR. Other indirect effects include complex microphysics interactions with atmospheric particles (such as ice nucleation, mixed-phase properties, hydrometeor size and fall speed) and exert positive or negative radiative forcing (Lohmann & Feichter, 2005). Moreover, changes in surface energy balance may impact temperatures and modify the atmospheric circulation and subsequently propagate the impact of aerosol perturbations globally (e.g. as Rossby waves) (e.g. Shindell et al., 2012). Circulation changes are also related to internal climate variability and impacted by other changes in the energy balance due to different forcings (greenhouse gases, land use change etc.), occurring on time-scales from days to decades. With such complex interactions between circulation and aerosols signals, the role of aerosols alone can be difficult to quantify.

Despite progress, there is still very large uncertainty in attributing observed regional-scale climate change to specific forcing factors and, particularly, in determining the contribution of aerosols (see Jones, Stott, and Christidis (e.g. 2013)). Understanding the relationships between aerosol emissions and associated radiative forcing and between radiative forcing and local and remote climate responses remains challenging. A large source of uncertainty, especially at regional scale, is due to internal variability in the atmospheric circulation (e.g. Shepherd, 2014). Transport, removal and internal variability on many timescales influence aerosol particle distributions (Gong et al., 2006) and cloud properties such that isolating statistically significant differences in radiative forcing due to an-

thropogenic aerosol perturbations typically requires integrating over long simulations, which can be prohibitively expensive.

Following these considerations, two questions arise:

1. How much do changes in aerosol emissions affect the local surface energy balance, given the observed atmospheric circulation?
2. What is the impact on recent regional temperature trends?

The traditional method for estimating simulated anthropogenic forcing is to compare two simulations (or ensembles) with and without anthropogenic emissions after integrating them over the timescales of the dominant modes of natural variability. In this case, the simulations not only have different emissions , but they are also unconstrained meteorologically, i.e., they produce circulation patterns that affect, for example, cloud cover and cloud liquid water content, the same properties involved with the aerosol indirect effect. A signal in the overall mean difference is only statistically significant where it is larger than a metric of internal variability (i.e., standard inter-annual error), and in practice the signal is often weak in those parts of the world where internal variability is high or the signal of aerosol effect is low.

Newtonian relaxation (nudging) techniques constrain the model evolution by relaxing the model toward a specified time-dependent dynamical state (Telford, Braesicke, Morgenstern, & Pyle, 2008). Therefore, the model dynamics (and thermodynamics) is to some extent controlled, resulting in synoptic variability similar to that observed and thus improving the realism of the model simulated atmospheric circulation state. This constrains the model variability (and biases) due to internal dynamics at the cost of damping circulation responses to aerosol forcing. This work takes advantage of this method to isolate the effect of the emissions alone: Numerical simulations are conducted with nudging of the winds to force the model dynamics to be similar in both runs while the aerosol emissions are different, and thus separate the local aerosol emission effect (LAEE) from the other potential feedback effects. The importance of the LAEE on the radiation budget (providing that the circulation is known) and temperatures is then investigated. The study makes a particular focus on East Asia and Europe, where a number of studies have suggested large aerosol changes have significantly modulated observed changes in regional climate during the 20th century (e.g. Dong, Sutton, & Shaffrey, 2017; Huang, Dickinson, & Chameides, 2006; Kasoar et al., 2016; Schultze & Rockel, 2017; Undorf et al., 2018).

Section 2 describes the nudging experiment and other datasets used. Section 3 presents key findings, and concluding remarks are provided in Section 4.

2 Methodology and data

2.1 Nudging experiment

The UK HadGEM Unified Model (UM) is used with its Global Atmosphere 6 component (Walters et al., 2017) at a N96 horizontal resolution (roughly 2°) and with 85 vertical levels. The historical sea surface temperature and sea ice from the Hadley Centre SST and sea ice dataset (Rayner et al., 2003) are prescribed. The model includes an aerosol scheme simulating processes for seven species: sulphate, mineral dust, sea salt, fossil fuel black carbon, fossil fuel organic carbon, biomass burning aerosols, secondary organic (biogenic). Further details of the aerosol scheme can be found in Walters et al. (2017).

Model zonal and meridional winds were nudged continually to winds taken from the ERA Interim dataset (ERAI, Dee et al. (2011)) with an update every 6 hours and with a relaxation coefficient of 4.629600e^{-05} (corresponding to the inverse of 6h $\times$ 3600s). Following the recommendation in Telford et al. (2008), nudging is not applied in the bound-

ary layer to avoid instabilities arising from differences between the UM and ERA-Interim model orography (below model level 12) or near the top of the model (above model level 82). Over open sea regions this corresponds to levels below 737 hPa and above 11 hPa respectively. Over high elevation areas (such as Himalayas) the correspondence in pressure levels can be different. Our nudging methodology is based on Telford et al. (2008) except we do not nudge the potential temperature, thus only the large scale circulation is forced.

Two simulations are carried out from September 1981 to December 2016. The first four months are considered as a spin-up and only the period January 1982-December 2016 is analysed. The first simulation (*HistAER*) uses full historical evolving emission for all aerosol species mentioned above (based on Lamarque et al. (2010) for the period up to 2005, and extended with the RPC4.5 emission scenario after) while the second (*ClimAER*) uses the 1982 emission (for all species) as a monthly climatology. None of the simulations include volcanic eruptions. The only difference between HistAER and ClimAER in terms of forcing is the evolution of aerosols emissions. As the aerosol feedback on the dynamics is limited by the nudging (except in the boundary layer) then by comparing the two simulations it is possible to estimate the LAEE.

Note that both runs use the same time-varying SST, sea ice and greenhouse gases concentrations (to be consistent with ERAI settings). Thus the aerosol feedback on the circulation is limited (e.g. Haywood et al., 2010). However, the model scheme allows aerosols to change the solar irradiance (direct effect) and hence the energy budget at the surface thereby changing surface temperatures which feed back onto fields such as relative humidity and hence precipitation formation. Cloud albedo is impacted by changes in cloud droplets properties (indirect effect). Both precipitation and cloud properties use parametrisation and are highly dependent on the model itself. Especially, cloud albedo responds directly to aerosol concentration locally (while precipitation is more controlled by dynamics and is expected to be limited by dynamics nudging). Both aspects can impact temperatures locally (though radiation changes for clouds and latent heat for precipitation) and are part of the LAEE on temperatures.. Also note that greenhouse gases concentrations are only considered as prescribed forcing here (no feedback or chemistry impact them directly). While we allow some of the climate response to aerosols to develop in the model, it is clear that only a portion of it is captured because of the use of prescribed SST and nudging in the free troposphere.

2.2 AOD changes and regions of interest

The evolution of aerosol concentration is illustrated by changes in total aerosol optical depth (AOD). Linear trend in AOD (during 1982-2016) in in HistAER is displayed in Fig. 1a, and supplementary Fig.S1 shows the AOD of individual species and time series of both simulations. The global mean AOD during 1982-2016 does not show a clear trend (about 0.0010 per decade) with only small differences between the two simulations. However, this near constant global average hides strong regional differences with increasing AOD over East Asia and decreasing AOD over Europe and North America (see also Undorf et al. (2018)), mainly due to changes in sulphate (SO_2) with small contributions from biomass burning (BioM) AOD. Sea salt also increases in both simulations over the Arctic region, presumably due to the reduction in sea-ice.

It is also noticeable that ClimAER has a small global positive trend for SO_2, that could be due to weather changes (especially water cycle, that can affect aerosol deposition, as shown by supplementary Fig.S3) and also climate-dependent oxidation processes that form aerosols in the atmosphere.

In the following, AOD corresponds to the sum of all aerosol individual optical depths. Four regions are identified where changes in total AOD are the largest: North-West USA

(US; 100°-60°W, 30°-45°N), Europe (EU; 5°W-45°E, 40°-60°N), India (70°-95°E, 15°-30°N) and East China (105°-125°E, 25°-40°N). We focus on these regions in the paper.

2.3 Reanalysis and observations

Several datasets used to compare against model outputs are listed below. They are also summarised in Table 1 with their acronyms.

- A network of surface shortwave radiation observations is used: The Global Energy Balance Archive (GEBA, Wild et al. (2017)). It has a global coverage but with different densities depending on the region (supplementary Fig.S2). Moreover, many stations have missing value or only a limited period of record. For this study, only stations with less than 20% missing values during the 1980-2014 period are selected. This sub-sampling leads to sparse coverage over North America and Asia. For this reason, the GEBA dataset is only used for the European region.
  To be more comparable with gridded datasets, sub-sampled stations are first converted into anomalies relative to their mean removing any local effects (for example, a station located in a valley would record less radiation than the regional averaged radiation). They are then gridded to the ERAI horizontal grid (through simple averaging over each grid point where observations are available). This dataset is only used to estimate the trends, not absolute values. Moreover, Wang (2014) and Wang, Ma, Li, and Wang (2015) showed that instrument sensitivity drift and instrument replacement in this datasets can lead to unreliable results. As no homogeneity control was performed in our study, results using GEBA dataset are considered cautiously.
- Another network of surface shortwave radiation observations is derived from observed sunshine duration over China (SSR_{obsCH}, Wang et al. (2015), Fig.S2d). Only stations with no missing record during 1980-2016 are used. The same gridding procedure as GEBA stations is applied for this network. The spatial and temporal coverage of this network is much denser than that of GEBA. This can be seen as a good indication to derive shortwave radiation from other observation networks (sunshine duration) when possible.
- Droplet effective radius observations derived from the National Aeronautics and Space Administration's (NASA) Moderate Resolution Imaging Spectroradiometer (MODIS) measurements (Platnick et al., 2015, 2017) are used as a reference for cloud properties. They cover the last 16 years of the period (2000-2016).
- Climate Prediction Center (CPC) global land minimum and maximum temperature gridded data, provided by NOAA (https://www.esrl.noaa.gov/psd/), are extracted for the period 1980-2016. As a complement, E-OBS dataset (Haylock et al., 2008) and regridded homogenised ground station observations (Li & Yan, 2009) are used for Europe and China region respectively.
- As ERAI is used as a reference for the dynamics of the model, results from the simulations are compared against ERAI variables (especially surface radiation and temperatures). Note that the model does not assimilate observations to constrain its surface temperature or other variables thus even with the same global dynamics than ERAI differences may arise (on top of aerosol signal).

2.4 Statistical significance tests

To test the robustness of trends a two-tailed t-test is used with variances estimated from the simulated interannual variability, where each year is considered as independent, and values above the 95% confidence level are considered as significant.

When comparing the mean states of the two simulations, we test two different aspects: Is the difference significant compared to the variability? And is the difference consistent from one year to another? The first is addressed by a two-tailed t-test (results are presented in Table 2). For the second we use a different approach as the year-to-year variability driven by dynamics is not independent. The year-to-year differences between the simulations are first computed. The mean difference over the period is significant at 95% level if it is above 2 standard deviation of the year-to-year differences scaled by the square root of the number of years. This method tests if the differences are consistent from one year to another.

3 Local aerosol emissions effect (LAEE)

This section presents the main results from the simulations. First, the effect of aerosol emissions on surface radiation and cloud properties is analysed. Then the responses in temperature and precipitation are presented.

3.1 Variations in radiation and cloud properties

Surface shortwave radiation (SSR) can be modulated both by atmospheric optical thickness and cloud cover. The first is related to both the absorption of gases (such as ozone) and aerosol concentrations, but as gases are the same in both simulations only aerosols will affect the differences in the nudged runs. Cloud cover is mainly due to the meteorology (humidity advection and condensation) so would expect little difference in cloud cover between the two simulations. However, cloud lifetime can also be locally modified by aerosols, and temperature changes can modify moisture condensation and cloud formation; both processes could produce changes in cloud cover between the two experiments. Moreover, intensity of incoming SSR at the top of the atmosphere depends on the season. To separate all these effects, clear sky radiation (i.e. radiation without cloud effect, SSR_{CS}) is first considered. Then actual SSR are analysed along with the changes in cloud properties. December to February (DJF) and June to August (JJA) seasons are considered separately.

The response in SSR_{CS} over the four regions is given in Fig.1b. As expected during summer SSR_{CS} increases over regions where AOD is decreasing in HistAER and vice versa, but remains near- constant in ClimAER and ERAI. During winter interannual variability is larger (probably due to more changing weather scattering aerosols) and differences between HistAER and ClimAER are relatively small. Some differences are however visible by the end of the simulations, especially over India (see Table 2 for significance test). During DJF incoming solar energy is smaller and meteorology variability is stronger so aerosol emission scenario has less impact on SSR_{CS}, especially over mid-latitude regions. In the following, we mainly focus on boreal summer, when SSR_{CS} differences are largest.

SSR (which includes effect of clouds) time series are shown in Fig.2. SSR Interannual variability is stronger than that of SSR_{CS} during JJA, especially over China and India highlighting the dominant role of the meteorology in controlling SSR variability (by cloud formation and aerosol scattering) that is similar in both simulations. Trend signs are in agreement with SSR_{CS} but with a weaker magnitude in ClimAER compared to HistAER which highlight the LAEE. Differences between the two simulations are however limited, except over Europe where they are significant. Model results (interannual variability and trends) are overall close to both *in situ* observations and reanalysis. Over China however, ERAI has a positive trend while HistAER shows a reduction in SSR. SSR_{obsCH} is more in agreement with the model and supports the robustness of simulation results for this region (Fig.2). Over EU the agreement between HistAER and GEBA is also clear, even with a scarce spatial coverage. Both ClimAER and ERAI underestimate the changes in this region. When looking at the full domain in the model outputs and ERAI (i.e. not

masked where observation are not available) similar results are found though the interannual variability is slightly weaker (not shown). This suggests that GEBA can represent the main trend in SSR over EU, but estimation of the interannual variability may be limited by the scarce coverage of the stations.

It is noticeable that radiation in both simulations and ERAI over India decreases. This is likely due to the impact of increased water vapour (from increased in SST). During winter differences between both simulations are less significant (Table 2), confirming the dominant role of the meteorology on the SSR variability and trend.

Significant mean differences between the two simulations for the last fifteen years (see section 2) are shown in Fig.3 for Asia and Fig.4 for US and EU. Changes in SSR are significant over China, India and EU, indicating that aerosol emissions likely reduced surface radiation over China and India and increased radiation over EU. Changes in SSR over the US are weaker but the increase in SSR is consistent with the decrease of HistAER emissions over this region. Thus the LAEE on SSR has a consistent long-term effect but is weak compared to the interannual variability (Table 2). On decadal timescales (not shown) variability is lower and differences between the two cases are significant for all regions, indicating that the long term effect of aerosol on radiation is not negligible. Similar results are observed during winter but with weaker impact on SSR over EU (Fig.S4 and S5).

Cloud properties are now analysed in terms of the cloud droplet effective radius (ERad) and total cloud cover (TCC). ERad changes in HistAER (Fig.2) are clear over all regions and consistent with the signal observed in SSR: Over China and India clouds become brighter (decrease in ERad) with increase in aerosols (thus decrease SSR), and the opposite for EU and US. This is also confirmed with ERad spatial patterns (Fig.3 and 4) being in agreement with SSR patterns. MODIS tends to have similar trends for Asia (decrease in ERad) but results are less clear for EU and US. Note that absolute values of ERad are about 8μm in the model and about 14μm in MODIS. Thus, clouds are too bright in the model and may have too strong an effect on SW radiation. Only weak differences in TCC are visible between HistAER and ClimAER which are not statistically significant. This suggests that the change in aerosols between the two simulations is not having a significant impact on TCC (which is mainly driven by meteorology) despite their impact on droplet properties. It indicates that if aerosols modify clouds lifetime or formation (as a feedback from temperature changes for example) it is not significant in the model compared to the meteorology control.

3.2 Temperatures and precipitation responses

The previous section showed the LAEE on surface shortwave radiation. For societal impact two important variables are considered: Temperature and precipitation. This section describes changes in daily maximum (Tmax) and minimum (Tmin) surface temperatures and then precipitation.

3.2.1 Temperatures

Significant positive differences in Tmax (about 0.5°C) is found for EU during summer (Fig.5), consistent with the decrease in aerosols emissions and increase in SSR over this region. This also leads to an increase in diurnal temperature range (DTR) as the response in Tmin is weaker. Over other regions no significant differences are found during summer. This is especially surprising for East Asia where clear signals were found for SSR. The base-model has shown to reliably simulate extreme temperatures seasonal signal over China (Freychet, Tett, Hegerl, & Wang, 2018) thus this absence of signal is unlikely due to a model bias. It is more likely that over China and India the large scale meteorology and induced local dynamics (which is the same in both simulations) have

larger control on temperatures. Also, as the SST is similar in both simulations, temperature advection from ocean over land is strongly constrained. The important conclusion is that the aerosol emissions impact on temperatures is weak here (despite previously noticed differences in SSR). The AOD-temperature changes relationship is investigated furthermore in Fig.6. It is clear that AOD differences are much larger in EU than over any other regions, which explains the stronger temperature response over EU. Even with weaker magnitude, both US and India follow same AOD-temperatures relationship than EU. On the other hand this relationship is less clear for China region, especially for Tmax during JJA (with Tmax changes being closer to zero or even slightly positive despite increase in AOD). Based on these results it is clear that significant temperature differences over EU are due to large AOD changes while temperature differences over China are limited by weaker AOD change and masked by other factors (such as local dynamics, advection or feedbacks) cancelling the AOD-temperature relationship. Finally, another hypothesis to explain the weak response over China would be to consider the possible effect of EU aerosols propagating to Asia: Providing that EU aerosols had an effect on cloud properties over China, then the effect of increasing Chinese aerosols could be compensated by the decrease in European aerosols, leading to a null or weaker change in cloud properties. This could explain for instance why ERad differences are not so strong over North-East China compared to SSR changes (Fig.3). This hypothesis could be tested by further work (by changing aerosol emissions over China and removing any aerosol emission over Europe for instance) but won't be investigated in this paper.

At global scale, aerosols emission scenario has only a weak consequences on temperatures, with a globally averaged land Tmax (Tmin) difference of about 0.03°C (0.005°C) between the two cases.

During winter, a clear reduction in Tmax is simulated over North India (Fig.5). Thus, during this season changes in SSR due to aerosol emissions have stronger effect on surface temperatures for this region. This reduction is also observed in China but the signal is not statistically significant. As expected, warming signals are also found over EU and US (but weaker compared to summer).

The LAEE on temperature trend (Fig.S6) is weak, with the largest differences between simulations being Tmax over EU, consistent with findings above. Signals in simulations are in accordance with ERAI (especially for EU and US) but agree less well with observations. Over China opposite signs are found: Negative in the model, positive in CH-OBS and CPC-OBS (in agreement with previous findings from Du, Wang, Wang, and Ma (2017)), neutral in ERAI. Many hypotheses could explain these differences (land-atmosphere heat and humidity exchange poorly represented in the model, station location...). The main message is that uncertainties between datasets (in terms of long term temperature changes) are in many locations larger than the LAEE in the model.

3.2.2 Precipitation

The impact on precipitation is now discussed (Fig.3 and 4 for summer, Fig.S4 and S5 for winter).

Precipitation tends to increase where aerosols decrease (US and EU) and decrease where aerosols increase (India and China). However, differences between simulations are overall not significant. Only North India shows a significant difference during summer where a reduction of 0.5 mm.day^{-1} in HistAER is observed.

This signal is related to a change in regional dynamics with a decrease in 500 hPa vertical velocity (in HistAER compared to ClimAER) along the Himalayas and West part of China (though any effect on vertical velocity is expected to be limited by control of horizontal circulation due to nudging, the model still has some freedom to adjust local the dynamics). This dynamical pattern and the moisture budget is exposed in Fig.S7.

The vertical velocity shows a dipole, with a strengthening over the Bay of Bengal (15°N) and a weakening at the foot of Himalayas (25°N). The horizontal moisture flux convergence (MFCh) also decreases over this area in the boundary layer (where no nudging is applied), leading to a reduction in total moisture flux convergence (MFC). Hence less moisture is available for precipitation. It is also noticeable that MFC increases near the surface but decreases at upper levels indicating shallower convection.

Based on the simulations, aerosol emissions are found to change precipitation significantly only over North India during the monsoon season, leading to a lower P-E budget. However this result must be considered carefully given the complex dynamical interaction between the low levels without nudging and the upper nudged levels. Part of the signal could be due to local model imbalance or instability. Over other region, differences between simulation are too weak to be considered significant.

The above results indicate that when dynamics and SST are prescribed the local impact of aerosol emissions on temperatures is small (except over Europe during summer and India during winter). Regions where AOD change is weaker and local dynamics or temperature advection may be more important (such as East Asia) may have a temperature variability dominated by the meteorology. In the same way, precipitation is found to be weakly impacted (except over North India during summer).

4 Concluding remarks

The role of local aerosol emissions on the surface radiation and regional climate was investigated using the UK HadGEM-GA6 model nudged to ERA Interim reanalysis. Two simulations were compared: One with the full historical aerosol emissions and another with a fixed monthly climatology aerosol emissions. The differences between the simulations gave an indication of the potential aerosol emissions effect.

The response in surface radiation was found consistent with aerosol changes (decrease in radiation where emissions increase and vice versa). It was also shown that in terms of interannual variability the signal can be strongly controlled by the meteorology, which may limit the detectability of aerosol impact.

Cloud droplet sizes responded quickly to aerosol emissions in the simulation. Some of this trends were also observable in MODIS data but the model clouds are found to be too bright. This, assuming no compensation between area and brightness, would lead to strong a cloud effect on surface radiation (with clouds reflecting radiation too strongly in the model).

The effect of aerosols on surface minimum and maximum temperatures was more nuanced. Temperatures over China were only weakly impacted despite a clear change in surface radiation. We hypothesize that dynamics is the dominant factor in this region (in the model) and over-shadows potential effects of radiation changes. It was also found that results from observation datasets show opposite trends, thus the model reliability (in terms of trends) over this region is questionable. More significant effects were found for the maximum temperature over India and EU with a decrease during winter and increase during summer respectively both consistent with aerosol concentration increase and decrease respectively.

Precipitation was not affected in the model except over North India and West China where a reduction of 0.5mm.day^{-1} was observed. Over other regions, the precipitation signal was not significant.

Based on these findings, the direct regional effect of aerosol emissions on temperature and precipitation cannot be considered as systematic or linear when the circulation and SSTs are not allowed to be modified by aerosols in the model. This is true es-

pecially in cases where dynamical variability is particularly large and dominates over the signal.

To understand more clearly the limited impact of aerosols over some regions (especially China) further work should be conducted. Especially, scaling the emission or AOD changes over each region so comparing their effect on temperatures would be more consistent and could provide an better understand on how much dynamics (from nudging) can control temperatures. Other experiments could also isolate effect of emission changes over regions one at a time, or removing aerosol emissions from other regions to quantify potential remote effect (for example the hypothesized European aerosols propagating effect over East Asia).

Nudging techniques such as employed for this work present several advantages. Forcing the circulation allows to compare easily different simulations and isolate specific signals (here the direct local aerosols impact). It also removes weather variability thus avoid the need of multi-member ensemble simulations. However one must keep in mind that results exclude potential feedbacks on the dynamics. Nudged observations and model physics should also be consistent or else it could lead to energy imbalance and unrealistic results.

Acknowledgments

This work was supported by the UK-China Research and Innovation Partnership Fund through the Met Office Climate Science for Service Partnership (CSSP) China as part of the Newton Fund (NF, ST). CPC Global Temperature data provided by the NOAA/OAR/ESRL PSD, Boulder, Colorado, USA, from their Web site at https://www.esrl.noaa.gov/psd/. We acknowledge the E-OBS dataset from the EU-FP6 project ENSEMBLES (http://ensembles-eu.metoffice.com) and the data providers in the ECA&D project (http://www.ecad.eu). We also would like to thank the reviewers for their valuable comments and efforts towards improving this manuscript.

References

Boucher, O., Randall, D., Artaxo, P., Bretherton, C., Feingold, G., Forster, P., ... Zhang, X. (2013). *Clouds and Aerosols. In: Climate Change 2013: The Physical Science Basis, Contribution of Working Group I to the Fifth Assessment Report of the Intergovernmental Panel on Climate Change [Stocker, T.F., D. Qin, G.-K. Plattner, M. Tignor, S.K. Allen, J. Boschung, A. Nauels, Y. Xia, V. Bex and P.M. Midgley (eds.)].* United Kingdom and New York, NY, USA: Cambridge University Press, Cambridge.

Dee, D. P., Uppala, S. M., Simmons, A. J., Berrisford, P., Poli, P., Kobayashi, S., ... Bechtold, P. (2011). The ERA-Interim reanalysis: Configuration and performance of the data assimilation system. *Quaterly J. of the Roy. Met. Soc.*, *137(656)*, 553-597.

Dong, B., Sutton, R. T., & Shaffrey, L. (2017). Understanding the rapid summer warming and changes in temperature extremes since the mid-1990s over Western Europe. *Clim. Dyn.*, *48(5-6)*, 1537-1554.

Du, J., Wang, K., Wang, J., & Ma, Q. (2017). Contributions of surface solar radiation and precipitation to the spatiotemporal patterns of surface and air warming in China from 1960 to 2003. *Atmo. Chem. and Phys.*, *17(8)*, 4931-4944.

Freychet, N., Tett, S. F. B., Hegerl, G. C., & Wang, J. (2018). Central-Eastern China persistent heat waves: Evaluation of the Amip models. *J. of Clim.*, *31(9)*, 3609-3624.

Gillett, N. P., Arora, V. K., Matthews, D., & Allen, M. R. (2013). Constraining the ratio of global warming to cumulative CO2 emissions using CMIP5 simula-

tions. *J. Climate*, *26(18)*, 6844-6858.

Gong, S. L., Zhang, X. Y., Zhao, T. L., Zhang, X. B., Barrie, L. A., McKendry, I. G., & Zhao., C. S. (2006). A simulated climatology of asian dust aerosol and its trans-pacific transport. part II: Interannual variability and climate connections. *J. Clim.*, *19(1)*, 104-122.

Haylock, M. R., Hofstra, N., Tank, A. K., Klok, E., Jones, P., & New, M. (2008). A european daily high-resolution gridded dataset of surface temperature and precipitation. *J. Geophys. Res (Atmospheres)*, *113*, D20119. doi: 10.1029/2008JD10201

Haywood, J. M., Jones, A., Clarisse, L., Bourassa, A., Barnes, J., Telford, P., & et al., N. B. (2010). Observations of the eruption of the sarychev volcano and simulations using the HadGEM2 climate model. *J. Geophys. Res (Atmospheres)*, *115*, D21.

Huang, Y., Dickinson, R. E., & Chameides, W. L. (2006). Impact of aerosol indirect effect on surface temperature over East Asia. *Proc. of the Nat. Ac. of Sc. of the United States of America*, *103(12)*, 4371-4376.

Jones, G. S., Stott, P. A., & Christidis, N. (2013). Attribution of observed historical near–surface temperature variations to anthropogenic and natural causes using CMIP5 simulations. *J. Geop. Res.*, *118(10)*, 4001-4024.

Kasoar, M., Voulgarakis, A., Lamarque, J.-F., Shindell, D. T., Bellouin, N., Collins, W. J., ... Tsigaridis, K. (2016). Regional and global temperature response to anthropogenic SO emissions from China in three climate models. *Atmos. Chem. Phys.*, *16*, 9785-9804.

Lamarque, J.-F., Bond, T. C., Eyring, V., Granier, C., Heil, A., Klimont, Z., ... van Vuuren, D. P. (2010). Historical (1850–2000) gridded anthropogenic and biomass burning emissions of reactive gases and aerosols: methodology and application. *Atmos. Chem. Phys.*, *10*, 7017-7039. doi: 10.5194/acp-10-7017-2010

Li, Z., & Yan, Z.-W. (2009). Homogenized daily mean/maximum/minimum temperatures series for China from 1960-2008. *Atm. and Oc. Sc. Let.*, *2(4)*, 237-243.

Lohmann, U., & Feichter, J. (2005). Global indirect aerosol effects: a review. *Atmos. Chem. Phys.*, *5*, 715-737.

Platnick, S., King, M. D., Meyer, K. G., Wind, G., Amarasinghe, N., Marchant, B., ... Riedi, J. (2015). MODIS Cloud Optical Properties: User Guide for the Collection 6 level-2 MOD06/MYD06 Product and Associated Level-3 Datasets. *Version*, *1*, 145.

Platnick, S., Meyer, K. G., Wind, G., Amarasinghe, N., Marchant, B., Arnold, G. T., ... Riedi, J. (2017). The MODIS Cloud Optical and Microphysical Products: Collection 6 Updates and Examples from Terra and Aqua. *IEEE T. Geosci. Remote*, *55*, 502–525. doi: 10.1109/TGRS.2016.2610522

Rayner, N. A., Parker, D. E., Horton, E. B., Folland, C. K., Alexander, L. V., & Rowell, D. P. (2003). Global analyses of sea surface temperature, sea ice, and night marine air temperature since the late nineteenth century. *J. Geophys. Res.*, *108*, 4407. doi: 10.1029/2002JD002670

Ribes, A., & Terray, L. (2013). Application of regularised optimal fingerprinting to attribution. part II: Application to global near-surface temperature. *Clim. Dyn.*, *41(11-12)*, 2837-2853.

Schultze, M., & Rockel, B. (2017). Direct and semi-direct effects of aerosol climatologies on long-term climate simulations over Europe. *Clim. Dyn.*, *50*, 3331-3354.

Shepherd, T. G. (2014). Atmospheric circulation as a source of uncertainty in climate change projections. *Nat. Geosc.*, *7(10)*, 703.

Shindell, D. T., Lamarque, J.-F., Schulz, M., Flanner, M., Jiao, C., & coauthors. (2012). Radiative forcing in the accmip historical and future climate simulations. *Atmos. Chem. Phys. Discuss.*, *12*, 21105-21210.

Stott, P. A., & Jones, G. S. (2012). Observed 21st century temperatures further con-

strain likely rates of future warming. *Atmosph. Sci. Lett.*, *13*, 151-156. doi: 10 .1002/asl.383

Telford, P. J., Braesicke, P., Morgenstern, O., & Pyle, J. A. (2008). Technical note: Description and assessment of a nudged version of the new dynamics Unified Model. *Atmos. Chem. Phys.*, *8*, 1701-1712.

Twomey, S. (1991). Aerosols, clouds and radiation. *Atmospheric Environment. Part A. General Topics*, *25(11)*, 2435-2442.

Undorf, S., Polson, D., Bollasina, M., Ming, Y., Schurer, A., & Hegerl, G. C. (2018). Detectable impact of local and remote anthropogenic aerosols on the 20th century changes of West African and South Asian monsoon precipitation. *J. of Geoph. Res.: Atm.*.

Walters, D., Boutle, I., Brooks, M., Melvin, T., Stratton, R., Vosper, S., ... Xavier, P. (2017). The Met Office Unified Model Global Atmosphere 6.0/6.1 and JULES Global Land 6.0/6.1 configurations. *Geosci. Model Dev.*, *10*, 1487-1520. doi: 10.5194/gmd-10-1487-2017

Wang, K. (2014). Measurement biases explain discrepancies between the observed and simulated decadal variability of surface incident solar radiation. *Scientific reports*, *4*, 6144.

Wang, K., Ma, Q., Li, Z., & Wang, J. (2015). Decadal variability of surface incident solar radiation over China: Observations, satellite retrievals, and reanalysis. *J. of Geo. Res.*, *120(13)*, 6500-6514.

Wild, M., Ohmura, A., Schär, C., Müller, G., Folini, D., Schwarz, M., ... Sanchez-Lorenzo, A. (2017). The Global Energy Balance Archive (GEBA) version 2017: A database for worldwide measured surface energy fluxes. *Earth System Science Data*, *9*, 601-613. doi: 10.5194/essd-9-601-2017

Table 1. Summary and acronyms of datasets used in the study.

Acronym	**Full name**	**Type**
ClimAER	Climatological Aerosols	Nudged model run (1982-2016) with repeating 1982 aerosol emissions each year.
HistAER	Historical Aerosols	Nudged model run (1982-2016) with historical aerosol emissions.
ERAI	ERA-Interim	Reanalysis (Dee et al., 2011).
GEBA	Global Energy Balance Archive	Surface shortwave radiation observation network (Wild et al., 2017).
SSR_{obsCH}	Chinese surface radiation network	Surface shortwave radiation observations derived from observed sunshine duration over China (Wang et al., 2015).
MODIS	Moderate resolution Imaging Spectroradiometer measurements	Satellite cloud droplet effective radius observation. (Platnick et al., 2015, 2017).
E-OBS	European Observation Network	Gridded land surface temperature observations over Europe (Haylock et al., 2008).
CH-OBS	Chinese Homogenised Temperature Network	Homogenised land surface station temperature observations for China region (Li & Yan, 2009).
CPC-OBS	Climate Prediction Center Temperature data	Global land minimum and maximum temperatures, provided by NOAA (https://www.esrl.noaa.gov/psd/).

Table 2. Regional mean differences during the 2002-2016 period for surface shortwave radiation (SSR), clear sky shortwave radiation (SSR_{CS}), maximum (Tmax) and minimum (Tmin) daily temperatures. Bold numbers indicate significant difference at 95% level (based on a t-test against the interannual variability). For each region, the first number is JJA and second is DJF.

	US	EU	China	India
SSR_{CS} ($W.m^{-2}$)	**3.7** / 1.1	**8.2** / 1.8	**-5.0** / **-2.6**	**-2.8** / **-2.9**
SSR ($W.m^{-2}$)	4.1 / 1.9	**11.0** / **3.1**	-3.3 / -1.9	-3.5 / **-2.8**
Tmax (°C)	0.23 / 0.18	0.47 / 0.29	0.001 / -0.10	-0.15 / -0.26
Tmin (°C)	0.13 / 0.09	0.23 / 0.19	0.08 / -0.06	-0.03 / -0.16

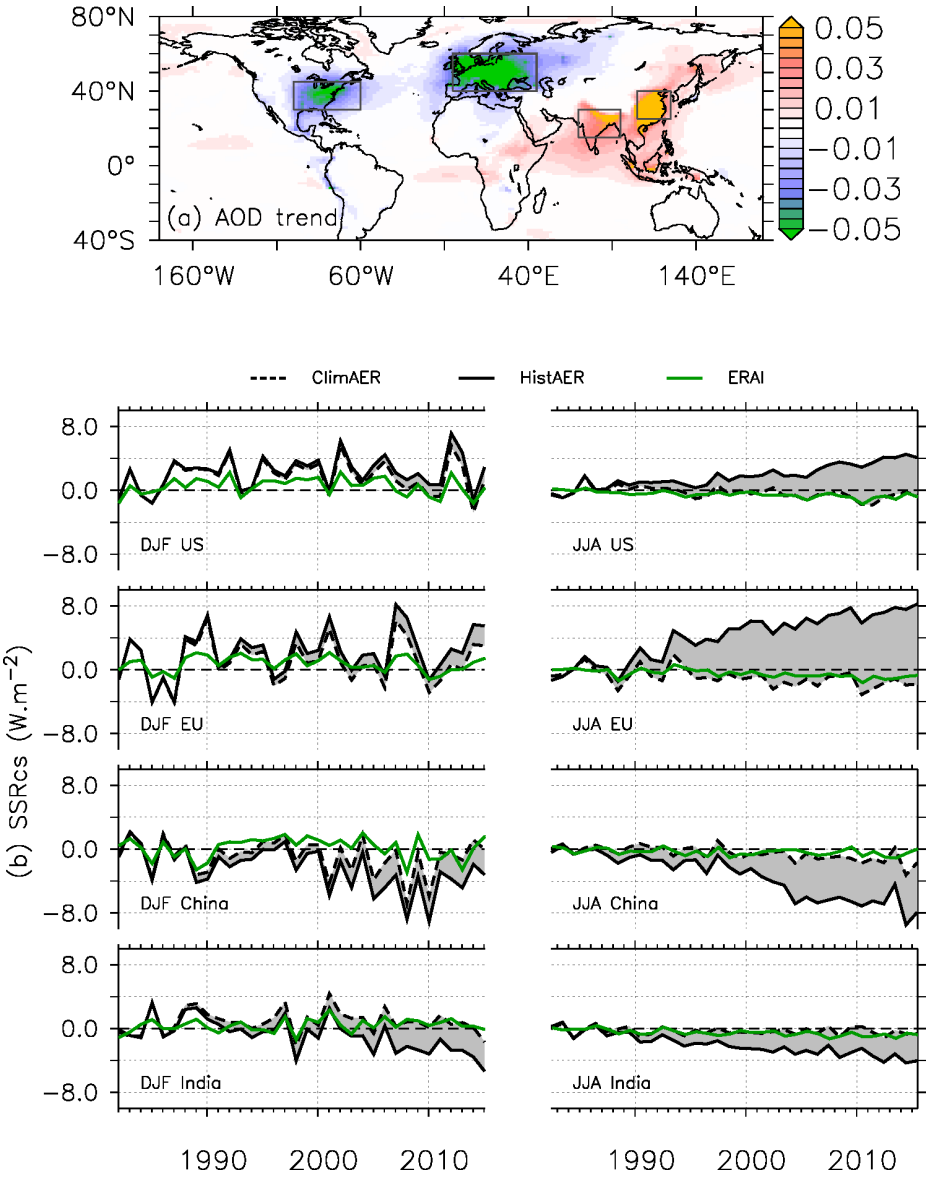

Figure 1. (a) Spatial change (per decade) in Aerosols Optical Depth (AOD, 550nm) for HistAER simulation. (b) Evolution of Surface Short-wave Radiation (SSRcs, W.m^{-2}) for HistAER (solid black line), ClimAER (dashed black line) and ERAI (solid green line). The grey shading highlights the difference between the two simulations. Time series are given for each region (black boxes in (a)) and two seasons: winter (DJF) and summer (JJA). Each series is plotted relative to the mean 1982-1992.

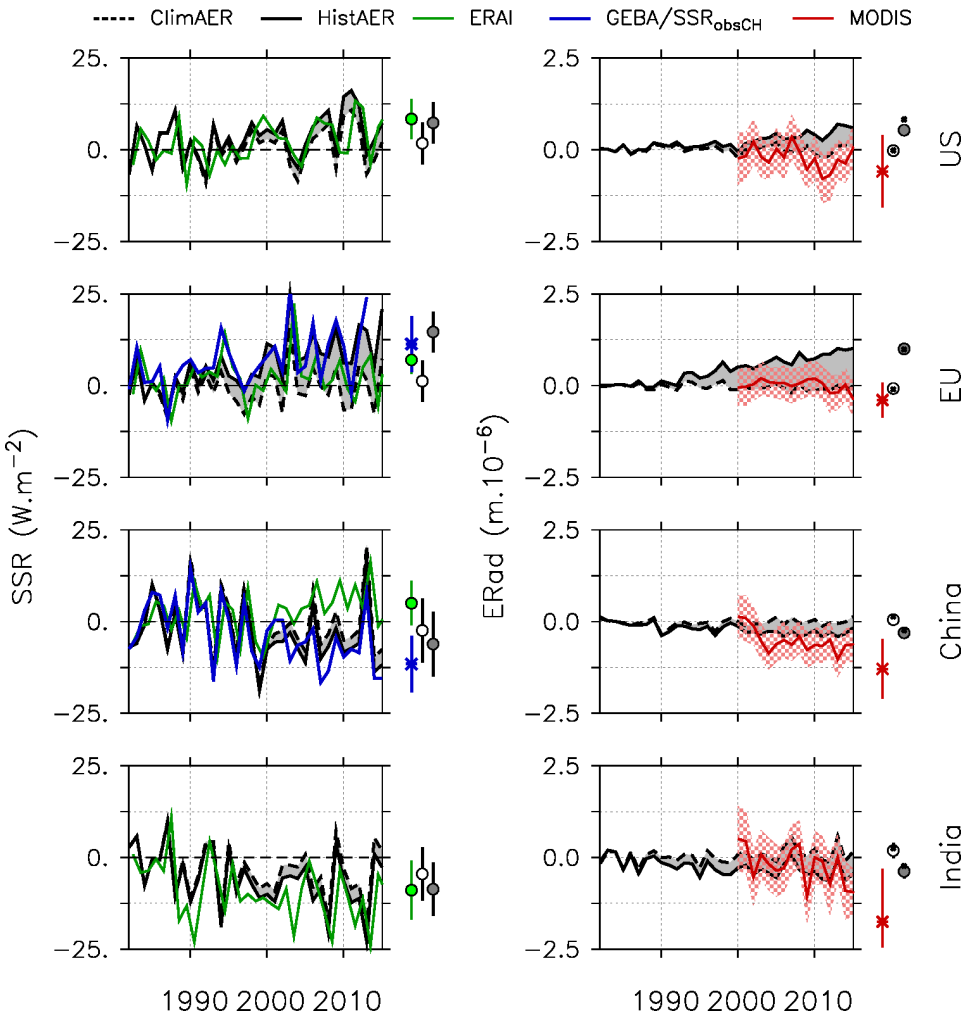

Figure 2. JJA evolution of net surface solar radiation (SSR, W.m^{-2}) and cloud droplet effective radius (ERad, μm). Solid and dashed black lines indicate HistAER and ClimAER respectively (with the grey shading highlighting the difference between the two simulations), the green line is ERAI and the red line is MODIS (with the grey shading being the uncertainties on the measurement). The dark blue lines represent GEBA stations for EU SSR and SSR$_{obsCH}$ for China SSR. Moreover for these two regions, HistAER, ClimAER and ERAI SSR is spatially masked where observation are not available.

All value are plotted as anomalies relative to the 1982-1992 mean, except for MODIS ERad which is given relative to the first 3 years of record (2001-2003). The symbols on the right of each sub-figure indicate the linear trends (per 3 decades, same scales as the time series) for HistAER (filled grey circle), ClimAER (empty circle), ERAI (green circle), MODIS (red star on ERad plots) and observations (blue stars on SSR plots). On ERad plot, a black cross for model also indicates the trend during the last 15 years (same period as MODIS). Vertical bars indicate the 95% confidence interval of the trends.

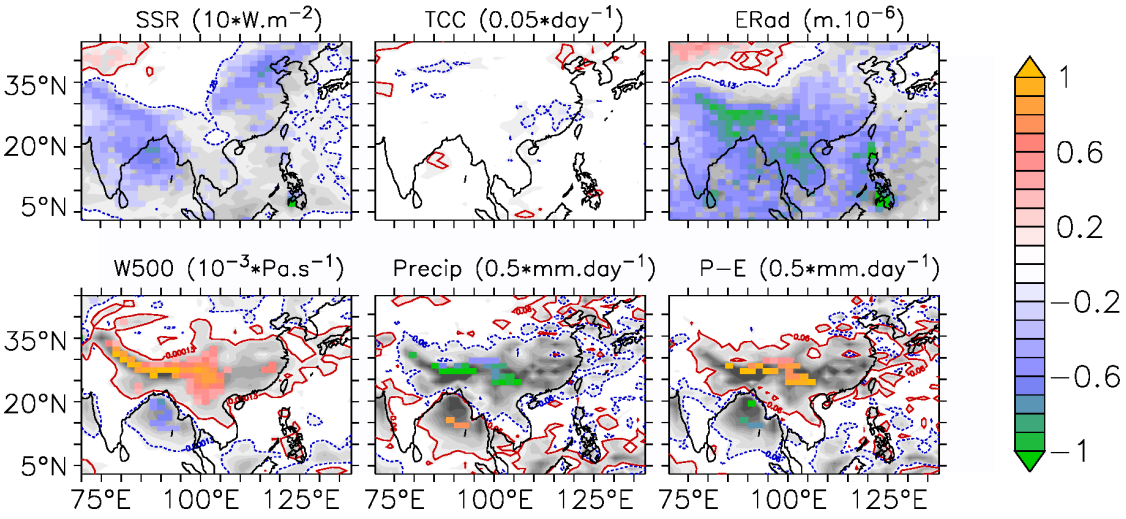

Figure 3. 2007-2016 simulated JJA difference (HistAER-ClimAER) for: surface net shortwave radiation (SSR, W.m^{-2}), total cloud cover fraction (TCC), cloud droplet effective radius (Erad, μm), vertical velocity at 500hPa (W500, Pa.s^{-1}), precipitation (Precip, mm.day^{-1}) and precipitation minus evaporation (P-E, mm.day^{-1}). The scale is shown in brackets for each variable (e.g. a difference of 1 in SSR indicates 10W.m^{-2}). Red and blue contours delimit area of positive and negative differences respectively (starting from 10% of the scales). Coloured area indicate significance level of 95%.

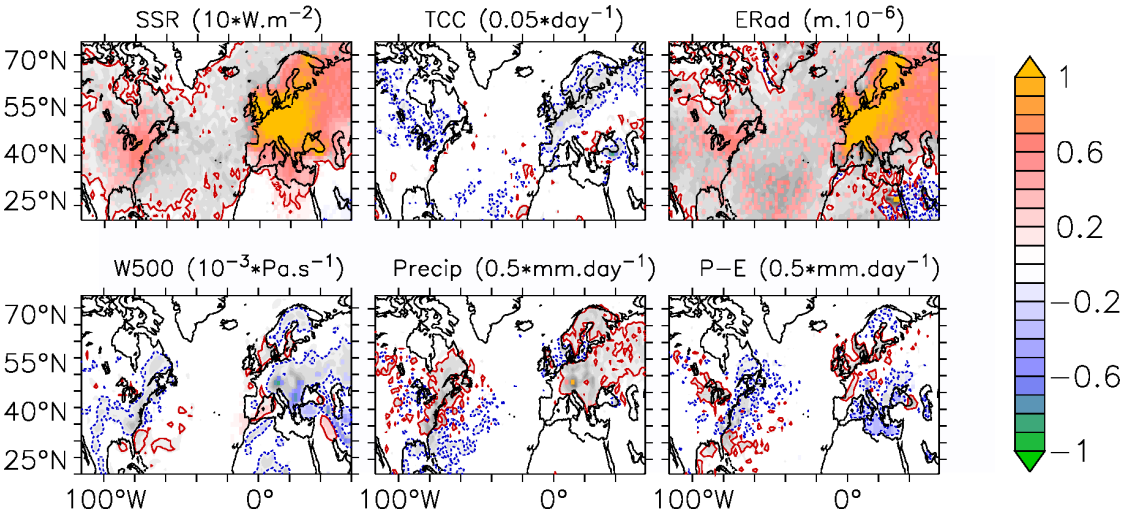

Figure 4. As Fig.3 but for North America and Europe regions.

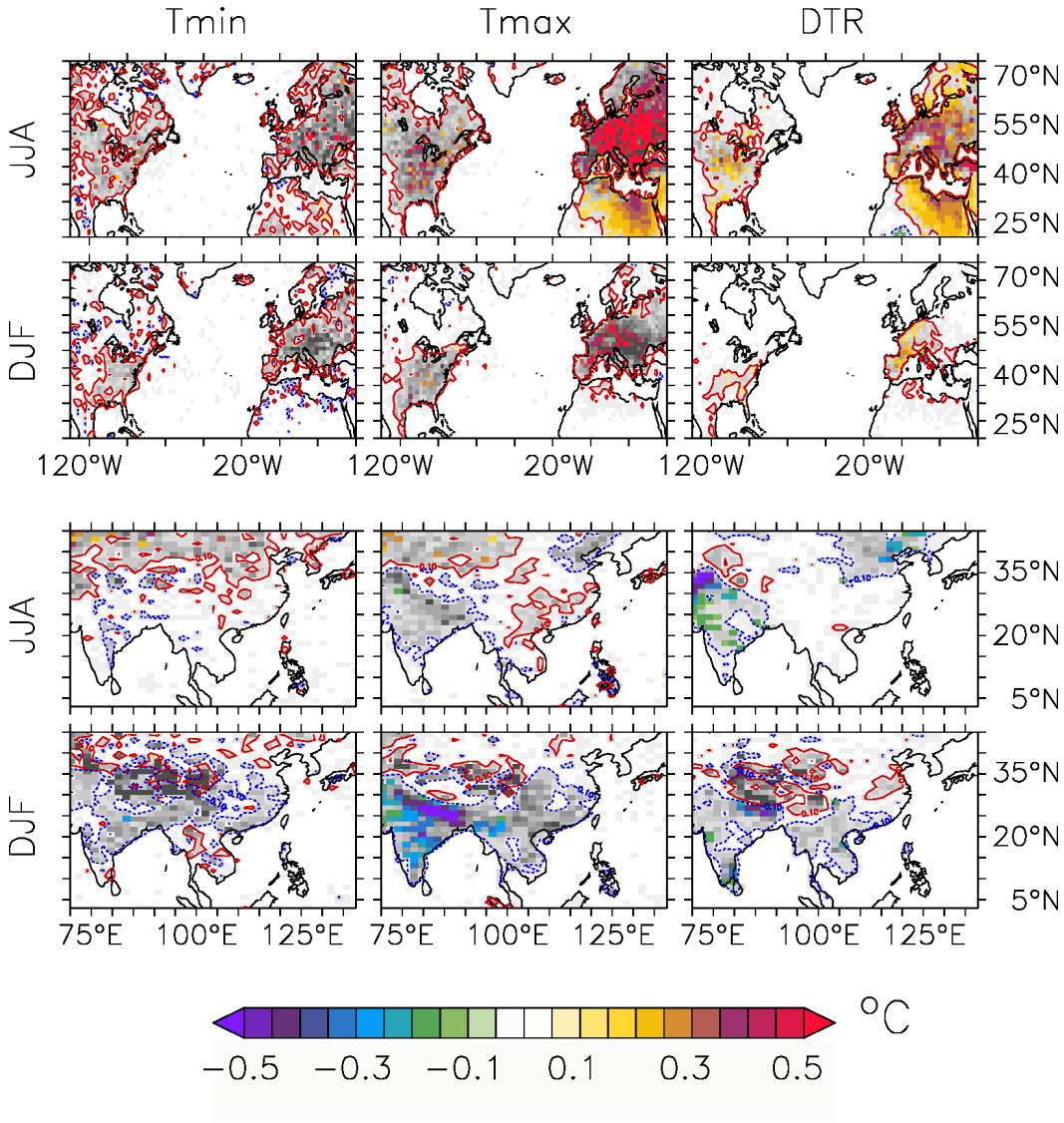

Figure 5. Difference (HistAER-ClimAER) in JJA mean daily minimum (Tmin) and maximum (Tmax) temperatures, and diurnal temperature range (DTR), for the 2002-2016 period. The upper and lower panel shows North America-Europe region and India-China region respectively, for both JJA and DJF periods. Red and blue contour highlight region of positive and negative differences respectively. All values are in °C. Only the area above the 95% confidence level is coloured.

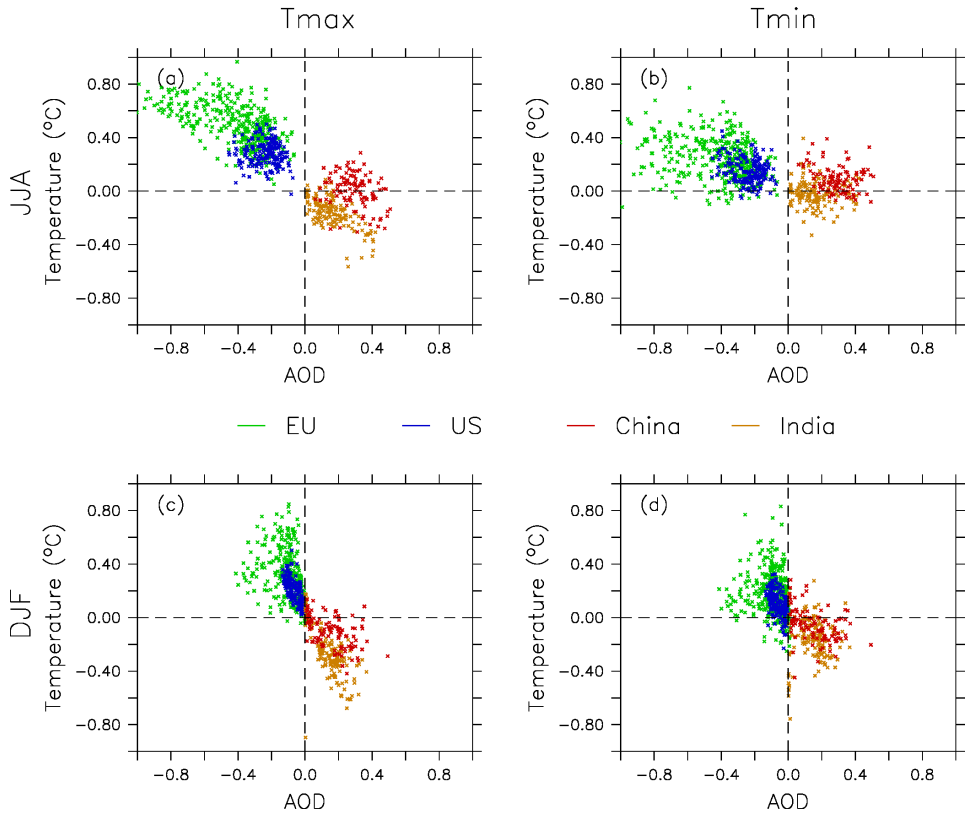

Figure 6. 2007-2016 simulated difference (HistAER-ClimAER) in AOD versus temperatures (Tmax and Tmin, in °C) at each grid point for the four regions: EU (green), US (blue), China (red) and India (orange). JJA and DJF seasons are separated.

Figure 1.

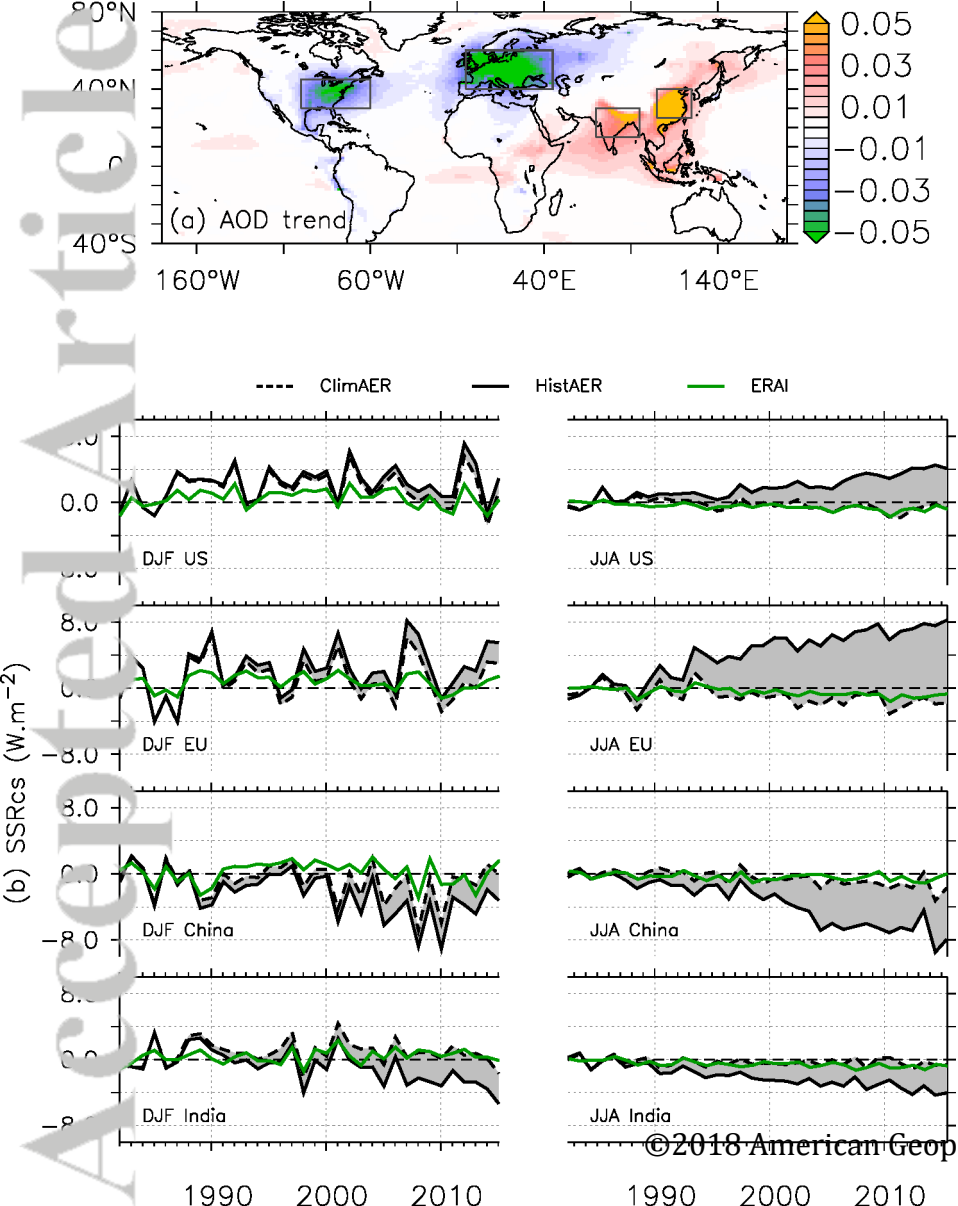

Figure 5.

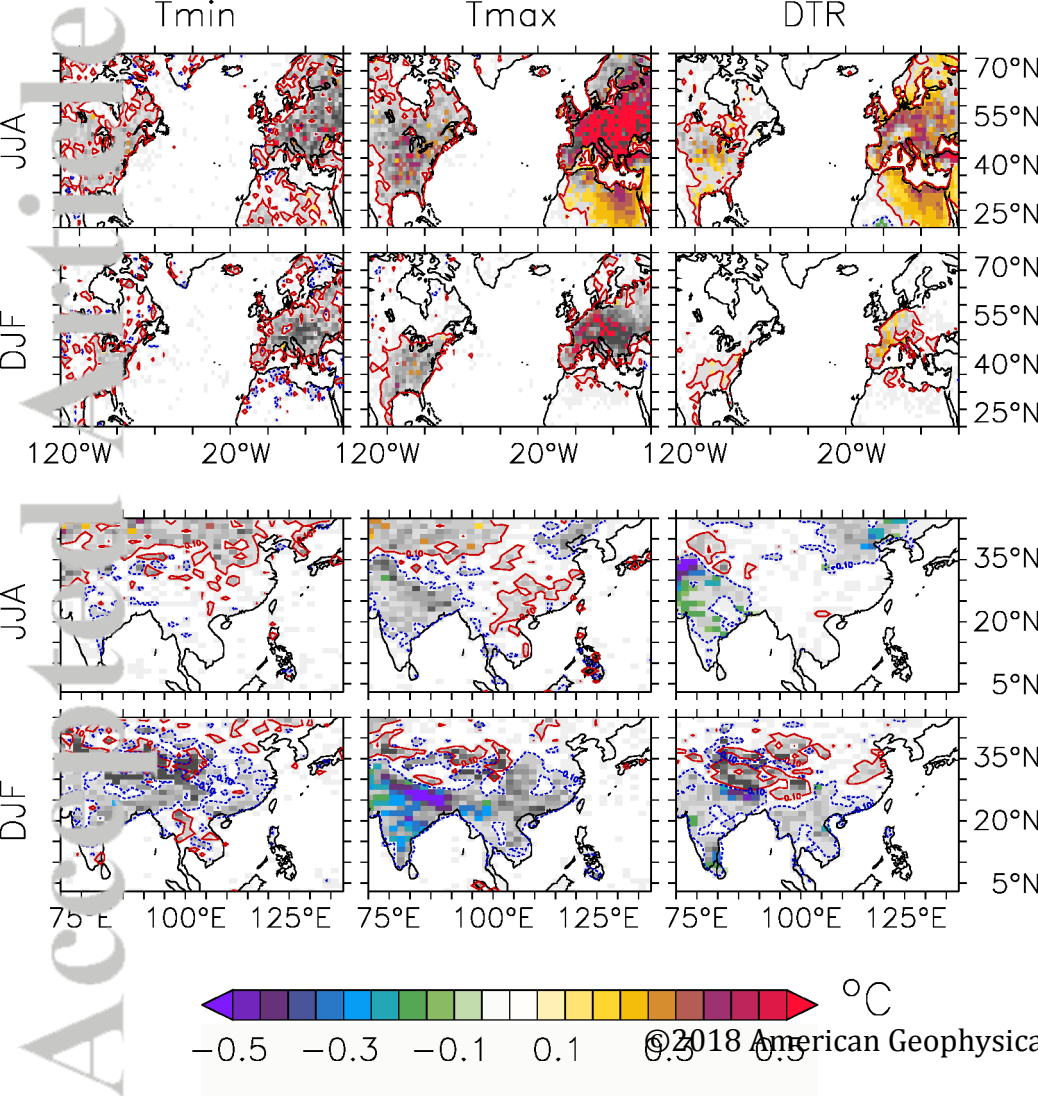

Figure 3.

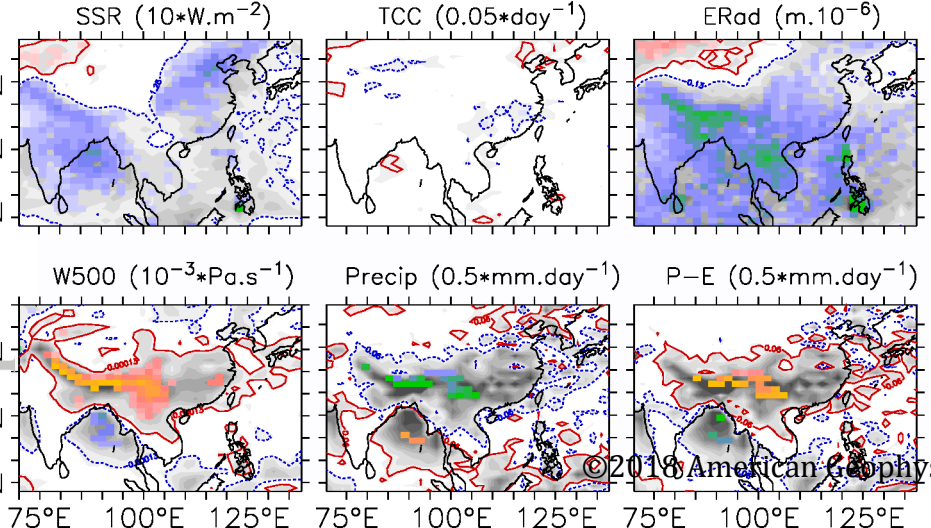

Figure 4.

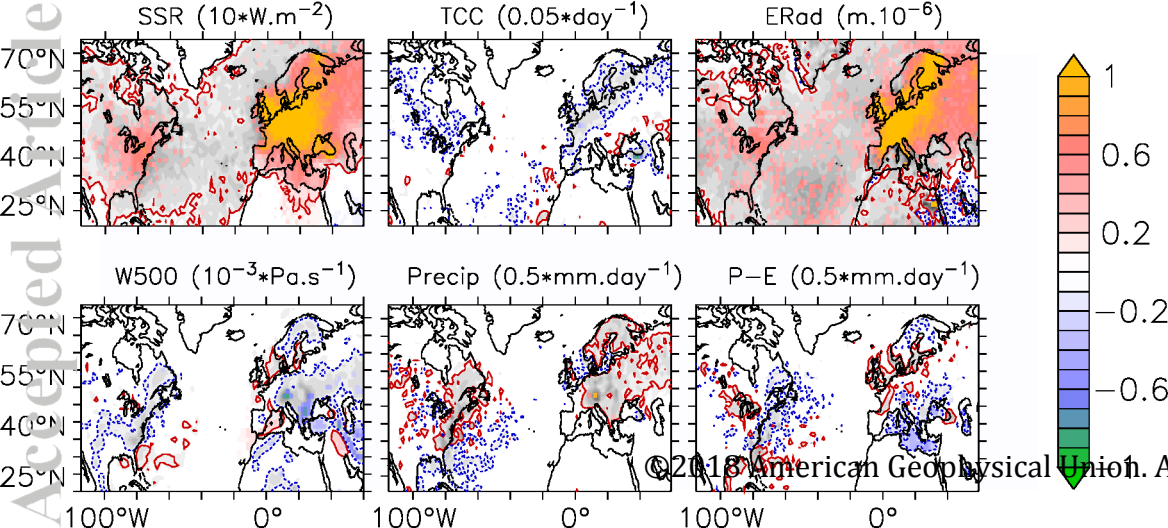

Figure 6.

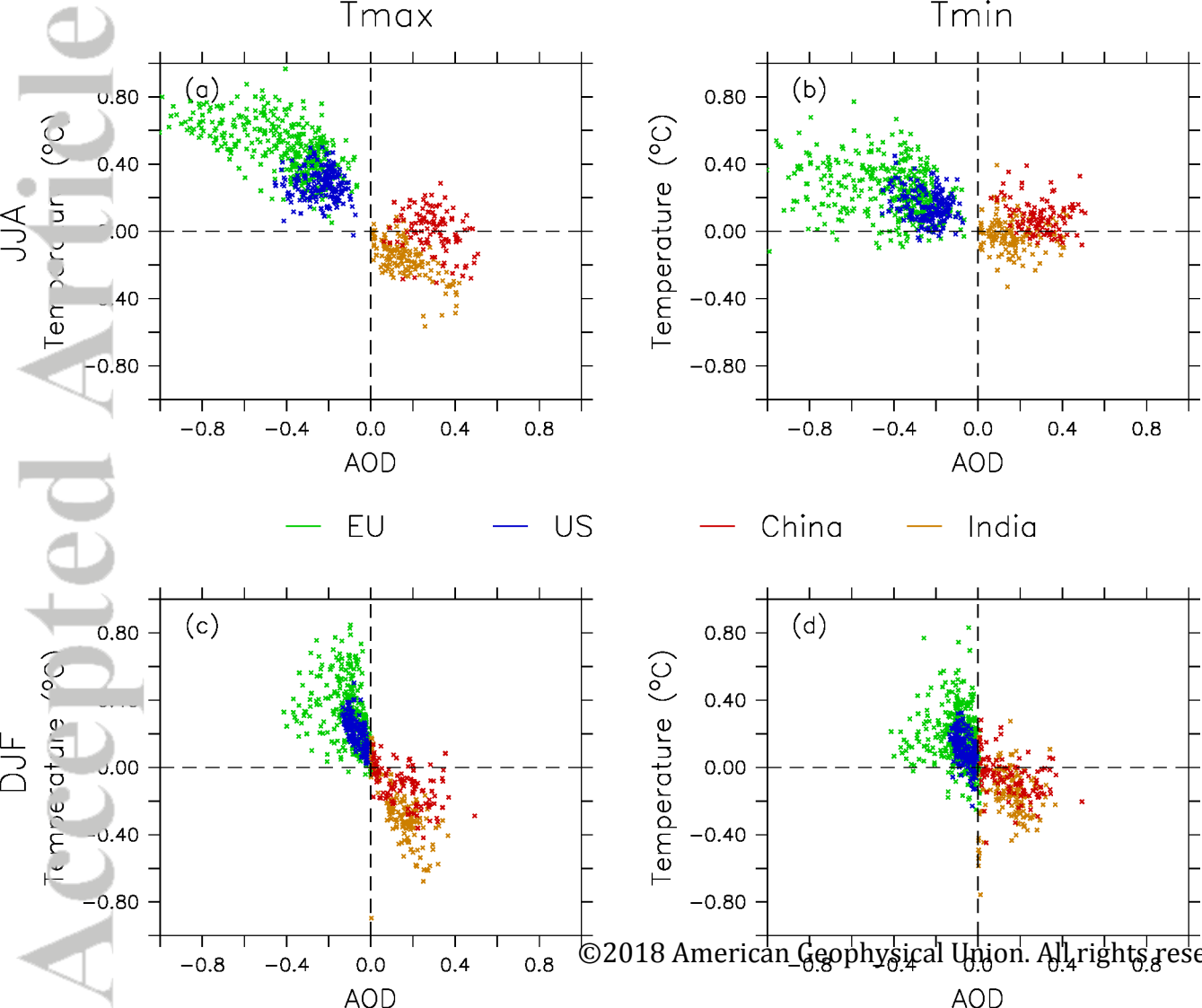

Figure 2.

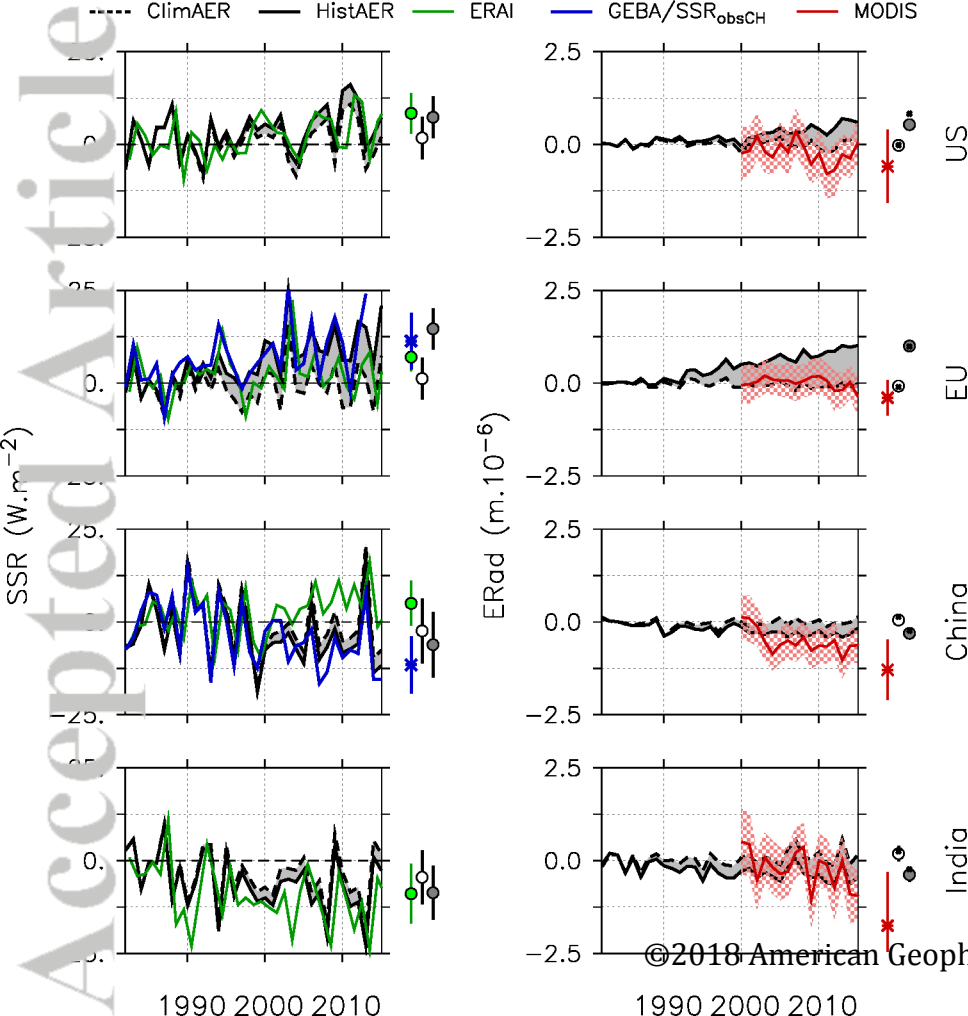

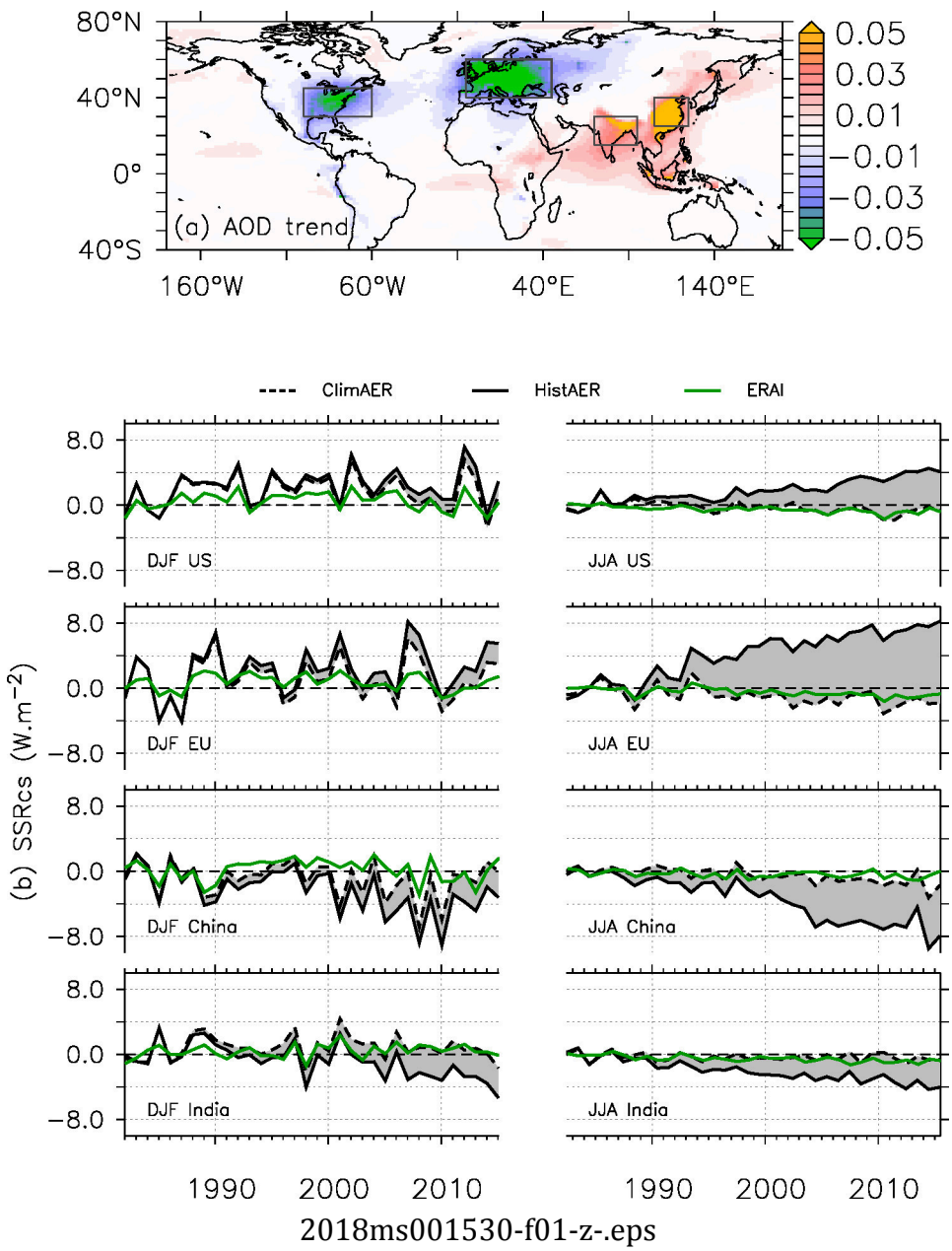

2018ms001530-f01-z-.eps

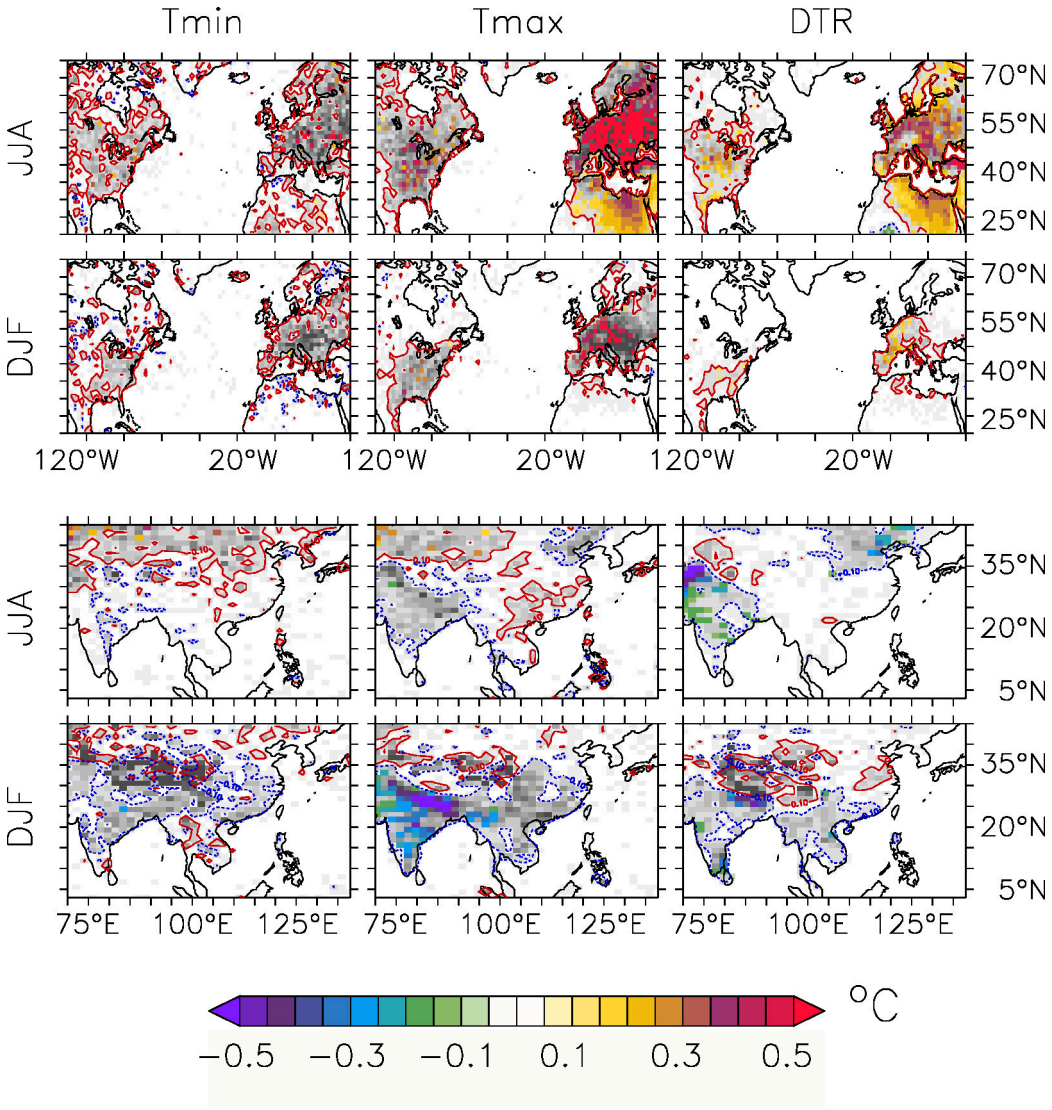

2018ms001530-f02-z-.eps

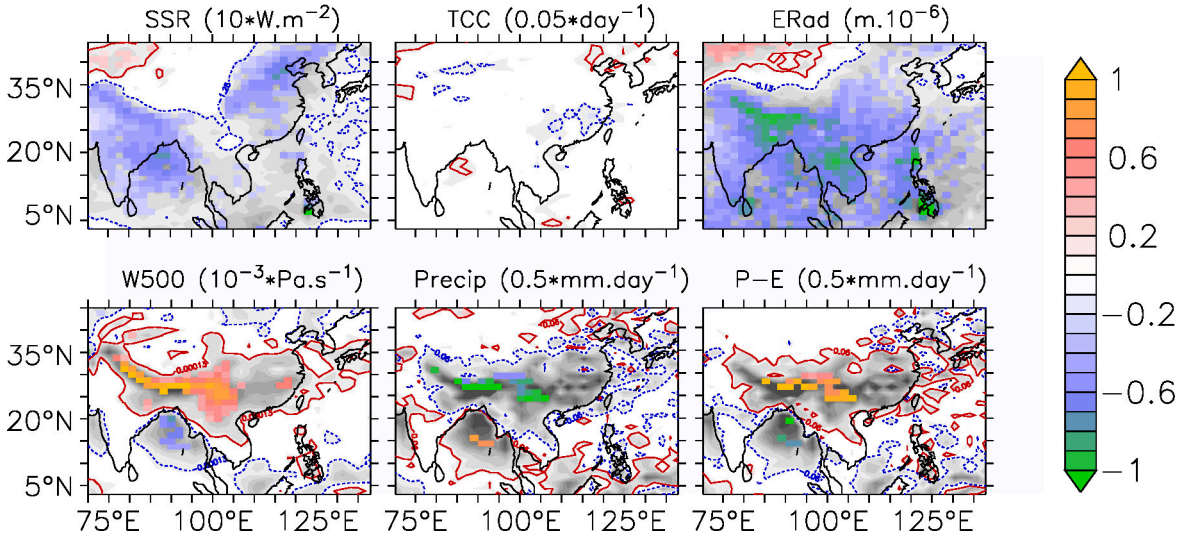

2018ms001530-f03-z-.eps

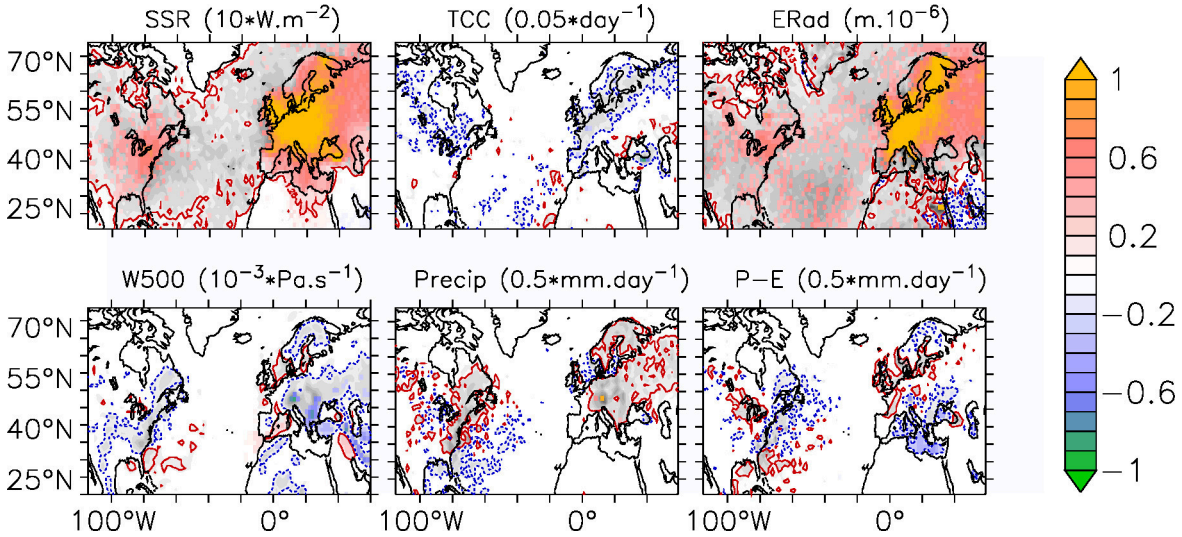

2018ms001530-f04-z-.eps

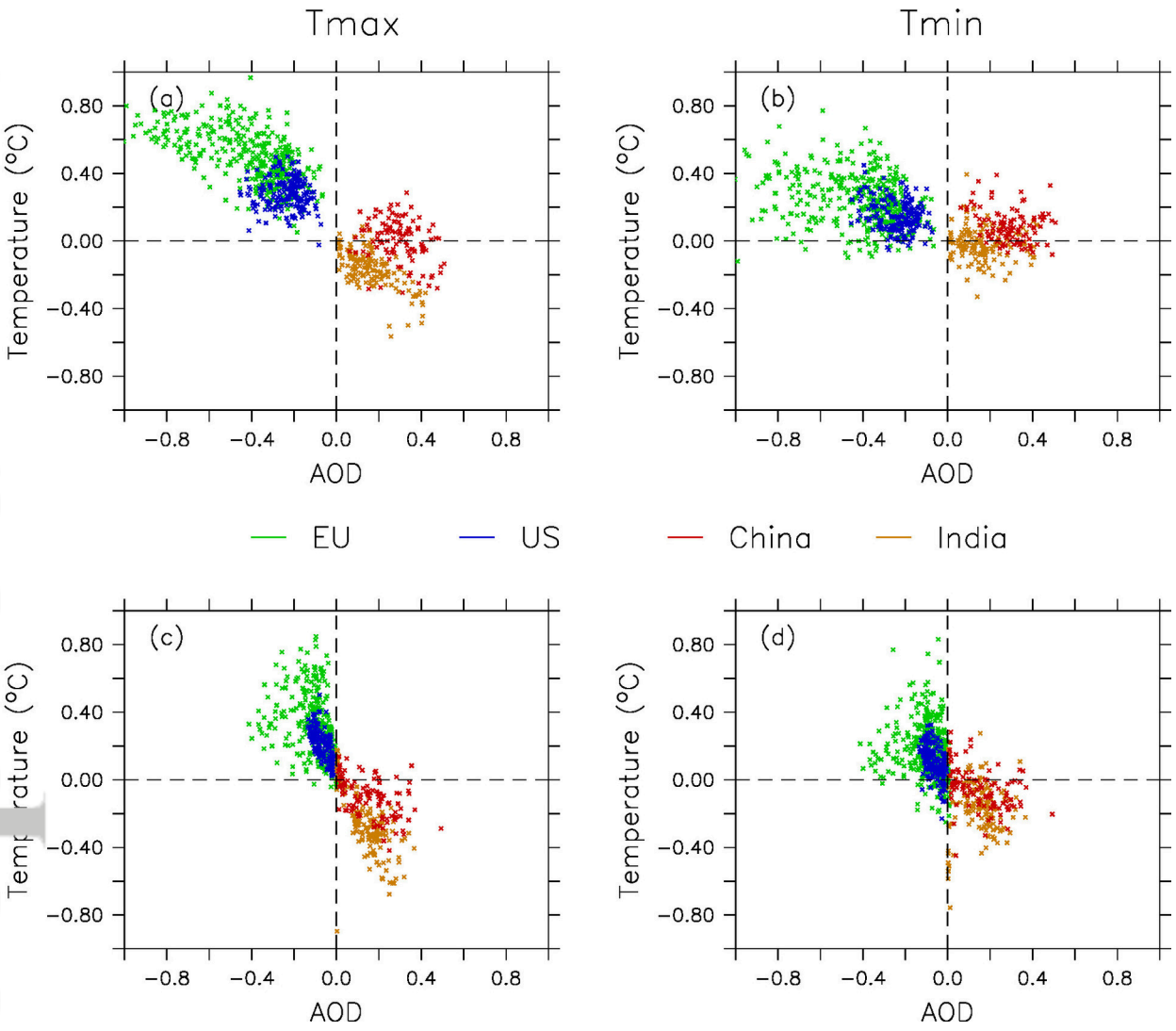

2018ms001530-f05-z-.eps